INTERNATIONAL JOURNAL FOR NUMERICAL METHODS IN FLUIDS, VOL. 22, 643–671 (1996)

# FINITE ELEMENT RESOLUTION OF CONVECTION–DIFFUSION EQUATIONS WITH INTERIOR AND BOUNDARY LAYERS

F. OLMOS

*Escuela de Empresariales, Universitat de Valencia, Artes Gráficas 13, E-46010 Valencia, Spain*

AND

F. CHINESTA AND R. TORRES

*Departamento de Mecánica de los Medios Continuos y Teoria de Estructuras, Universidad Politécnica de Valencia, Camino de Vera S/N, E-46071 Valencia, Spain*

SUMMARY

The purpose of this paper is to present a new algorithm for the resolution of both interior and boundary layers present in the convection–diffusion equation in laminar regimes, based on the formulation of a family of polynomial–exponential elements. We have carried out an adaptation of the standard variational methods (finite element method and spectral element method), obtaining an algorithm which supplies non-oscillatory and accurate solutions. The algorithm consists of generating a coupled grid of polynomial standard elements and polynomial–exponential elements. The latter are able to represent the high gradients of the solution, while the standard elements represent the solution in the areas of smooth variation.

KEY WORDS: spectral and finite elements; polynomial-exponential elements; boundary layers; connection–diffusion

## 1. INTRODUCTION

In convection–diffusion problems, when the convective term dominates the diffusive term, boundary and interior layers can appear due either to the boundary conditions or to the source term. Obtaining a good representation of these boundary layers by means of numerical methods has been a main focus of activity for some time, since when the diffusion $D$ tends towards zero, several oscillations (without physical meaning) appear in the solutions supplied by centred schemes.[1] The Galerkin formulation of finite elements avoids this problem by imposing restrictions on the size of the elements placed in the boundary layer. In spectral techniques (spectral elements) it is necessary to increase the order of polynomial interpolation inside the boundary layer. This requires either a geometrical non-conforming formulation (mortar elements) or a coupling with finite elements in order to avoid an excessive number of degrees of freedom.[2–4]

To solve the above problems, several methods have been developed. In spectral techniques the Galerkin formulation is neglected within the zone of the boundary layer by using a mixed spectral element method–collocation method.[5] In the case of the finite element method the streamline upwind Petrov–Galerkin technique is the method with the best properties.[1,6–9]

In this paper we present a new finite element technique to solve the two-dimensional steady convection–diffusion equation. The method is based on the following two ideas.

1. The behaviour of the solution within the boundary layer zone can be simulated using exponential functions.[10]

CCC 0271–2091/96/070643–29

*Received 21 July 1993*
*Revised 11 May 1995*

2. This exponential behaviour can be represented by an adequate basis of exponential functions.

The technique is basically a Galerkin finite element method modifying locally the basis of the space of approximation $X_h$ from information concerning the placement and behaviour of the boundary layers. It involves making a structured mesh such that the directions of high gradients in the solution coincide with the boundary of some mesh elements. In this mesh the bases of elements located in the zone of the boundary or interior layer are modified, whereas the bases of the other elements are preserved.

In order to explain the technique, we can start with a one-dimensional example allowing us to establish the main features of the method.

## 2. STATEMENT OF THE PROBLEM

### *2.1. A unidimensional example*

Consider the unidimensional convection–diffusion equation

$$\begin{aligned} -D\frac{d^2\phi}{dx^2} + v\frac{d\phi}{dx} &= k\delta(x-1), \quad x \in ]0, 2[, \\ \phi &= 0, \quad x = 0, \\ \frac{d\phi}{dx} &= 0, \quad x = 2. \end{aligned} \tag{1}$$

The local behaviour of the solution of equation (1) can be studied near the source term by isolating the interval $]1-\varepsilon, 1[$ and solving the equation

$$-D\frac{d^2\tilde{\phi}}{dx^2} + v\frac{d\tilde{\phi}}{dx} = 0, \quad x \in ]1-\varepsilon, 1[. \tag{2}$$

We take as boundary conditions

$$\tilde{\phi}(1-\varepsilon) = 0 \tag{3}$$

for appropriate $\varepsilon$ and

$$\tilde{\phi}(1) = K, \tag{4}$$

where $K$ is the unknown value at $x=1$ of $\phi$ in equation (1). The solution of equation (2) is given by

$$\tilde{\phi} = A + Be^{(v/D)x}, \tag{5}$$

with $A$ and $B$ having values which depend on the boundary conditions. Therefore, if $v$ dominates $D$, the solution of equation (1) presents a high gradient around the point $x=1$. In the following we will explain how information about the local behaviour of the solution can be used in order to obtain a good representation of the interior layer.

Consider the grid formed by two elements $\Omega^1 = [0, 1]$ and $\Omega^2 = [1, 2]$. Notice that we have made the upper edge of the first element $\Omega^1$ coincide with the point where the interior layer is located. Let the space of approximation be

$$\tilde{X}_h = \left\{ v \in C^0([0,2]) / v|_{\Omega^1} \in \langle 1, e^{p(x-1)} \rangle;\ v|_{\Omega^2} \in \langle 1, x \rangle;\ v(0) = 0;\ \frac{dv}{dx}(2) = 0 \right\}, \tag{6}$$

where $\langle f_1(x), f_2(x)\rangle$ denotes the vectorial subspace generated by two functions $f_1$ and $f_2$. Let

$$a(\phi_h, \Psi_h) = D\int_0^2 \frac{d\phi_h}{dx}\frac{\Psi_h}{dx} + v\int_2^0 \frac{d\phi_h}{dx}\Psi_h. \tag{7}$$

Thus the Galerkin formulation in $\tilde{X}_h$ will be: find $\phi_h \in \tilde{X}_h$ such that for all $\Psi_h \in \tilde{X}_h$,

$$a(\phi_h, \Psi_h) = k\Psi(1). \tag{8}$$

Starting from equation (8) and the above boundary conditions, we obtain the solution in $\tilde{X}_h$ as

$$\phi_h = \begin{cases} \dfrac{k}{v}(e^{p(x-1)} - e^{-p})\dfrac{1}{1-e^{-p}}, & x \in \Omega^1, \\ \dfrac{k}{v}, & x \in \Omega^2. \end{cases} \tag{9}$$

The analytic solution of problem (1) is given by

$$\phi(x, \zeta_0) = \begin{cases} \dfrac{k}{v}(e^{(v/D)(x-\zeta_0)} - e^{-(v/D)\zeta_0}), & x \geqslant \zeta_0, \\ \dfrac{k}{v}(1 - e^{-(v/D)\zeta_0}), & x > \zeta_0, \end{cases} \tag{10}$$

with $\zeta_0 = 1$ being the point where the source is placed. Therefore we are able to make an analysis of the error.

Taking into account that $e^{-v/D}$ and $e^{-p}$ are negligible, we have $1 - e^{-p} \approx 1$, $1 - e^{-v/D} \approx 1$ and $e^{-(v/D)(x-1)} - e^{-v/D} \approx e^{-(v/D)(x-1)}$. Then

$$\|\phi - \phi_h\|_{L^2} \approx \frac{k}{v}(\|e^{(v/D)(x-1)} - e^{p(x-1)}\|_{L^2}) \tag{11}$$

and

$$\|\phi - \phi_h\|_{H^1} \approx \frac{k}{v}\left(1 + p - \frac{v}{D}\right)(\|e^{(v/D)(x-1)} - e^{p(x-1)}\|_{L^2}). \tag{12}$$

Therefore the $L^2$ and $H^1$ errors of the solution are of the order of the approximation error of the exponential $e^{(v/D)(x-1)}$ by $e^{p(x-1)}$, i.e.

$$\|\phi - \phi_h\|_{L^2} = O(\|e^{(v/D)(x-1)} - e^{p(x-1)}\|_{L^2}) \tag{13}$$

and

$$\|\phi - \phi_h\|_{H^1} = O(\|e^{(v/D)(x-1)} - e^{p(x-1)}\|_{L^2}). \tag{14}$$

Thus the accuracy of the $\tilde{X}_h$ solution depends on an accurate approximation of the exponential $e^{(v/D)(x-1)}$.

By using the information supplied by problem (2), it is possible to obtain the order of the exponential to place in the basis of element $\Omega^1$ in order to get an accurate solution of problem (1).

### *2.2. Introduction to the bidimensional problem*

Generalization of the former case to the bidimensional case is not evident and this is the aim of the present study. Firstly we will define the hypothesis and notation to be assumed.

*Notation and hypotheses*

Let $\mathbf{v}$ be a field of velocities in an open subset $\Omega \in \mathbb{R}^2$ with regular boundary $\partial\Omega \equiv \Gamma$. The inflow boundary will be denoted by $\Gamma_- = \{x \in \Gamma : (\mathbf{v}, \mathbf{n}) < 0\}$, where $\mathbf{n}$ is the outward unit normal to $\Gamma$. $\Gamma_+ = \{x \in \Gamma : (\mathbf{v}, \mathbf{n}) > 0\}$ will be the outflow boundary and $\Gamma_0$ the set $\{x \in \Gamma : (\mathbf{v}, \mathbf{n}) = 0\}$.

Units are SI units unless otherwise specified.

The convection–diffusion equation

$$-D\Delta\phi + \mathbf{v}\nabla\phi = f(x, y) \tag{15}$$

is considered. $\Gamma_D$ will be the zone of the boundary $\Gamma$ with Dirichlet boundary condition and $\Gamma_N$ will be the zone with Neumann condition.

Two hypotheses are assumed.

1. The vectorial field of velocities $\mathbf{v}(x, y)$ is known and derives from the resolution of either a scalar potential or an incompressible viscous flow problem.
2. The source term does not affect the streamlines of the velocity field.

As in the one-dimensional case, the weak variational Galerkin formulation of the equation has been considered:

$$\int_\Omega (D\nabla\phi_h \nabla\Psi_h + v\nabla\phi_h\Psi_h) = \int_\Omega f\Psi_h. \tag{16}$$

Generalization of the method shown in the above example requires answers to the following questions.

1. How does one make up a grid which locates the boundary layers?
2. How does one modify the space of approximation $X_h$ by introducing exponential functions in the basis in order to simulate the behaviour of the boundary layers?

The starting point must be the knowledge of the behaviour and situation of the boundary layers. In the following section we present a brief summary of the main classical results concerning this subject, which will be used as the base for the construction of a structured mesh made up of quadrangular elements able to locate the boundary layers. Section 4 covers this subject. In Section 5 we present the modifications which are required in order to define a new approximation space $\tilde{X}_h$. In Section 6 we cover the problems of the calculation of shape functions and the attainment of quadrature formulae necessary to establish the algebraic system of equations. Finally, in Section 7 we summarize the main steps of the algorithm. Moreover, a numerical study of the properties of the method will be made through a set of test problems.

## 3. RESULTS CONCERNING BOUNDARY LAYERS IN BIDIMENSIONAL PROBLEMS

There is a specific bibliography about the interior and boundary layers in convection–diffusion problems.[11–13] In this section we sum up the main outcomes concerning this topic, which have been used in the following sections in order to make up structured grids and set up the functions that simulate the behaviour of the solutions in the boundary layer. The main characteristics of boundary layers in which we are interested are

(i) their spatial location
(ii) directions with high gradients in the solution
(iii) the width of interior and boundary layers.

To study the width of a boundary layer, we assume that the field of velocities is referred to a local curved co-ordinate system $(s, t)$, where the $s$-direction is the streamline direction and the $t$-direction is orthogonal to the streamline direction. If the velocity $\mathbf{v}$ is $(v_x, v_y)$ referred to Cartesian axes, we can assume $\mathbf{v} = (|v|, 0)$ as a linear approximation of $\mathbf{v}$ in the $(s, t)$ system.

*Interior layers generated by an interior source point*

An interior source point generates an interior layer in a nearly circular region around this point in the streamline direction, its size being $O(D/v)$. Downstream from this point an internal layer develops along the streamline in the orthogonal direction, its width being $O(\sqrt{(rD/v)})$, where $r$ is the distance downstream from the source point.

*Interior layers generated by a boundary condition*

If a boundary layer develops owing to a boundary condition, it can be located in a neighbourhood of the part of the boundary which generates it. If the outflow boundary $\Gamma_+$ generates the boundary layer, then the directions of the high gradients are the streamlines. The width of an outflow boundary layer is $O(D/v)$. If the boundary layer is generated by a tangential boundary, the directions of the high gradients are orthogonal to the streamlines. In this case the boundary layer is parabolic in profile, with thickness $O(\sqrt{(Dr/v)})$, where $r$ is the distance along the tangential boundary.

*Interior layers generated by a distributed source*

The streamlines passing through a distributed source produce a shadow zone downstream, developing an interior layer containing this area. The behaviour of the interior layer is similar to the above cases.

*3.1. How to simulate a boundary layer by means of an exponential function*

Knowledge of the width of the boundary layer allows us to compute the exponent of an exponential function simulating this behaviour.

Let $\delta$ be the width of the boundary layer developing along a streamline, measured on a line orthogonal to the streamline. Around the zone of the boundary layer we consider a linear approximation of this line. In local co-ordinates $(s, t)$ this line can be mapped into the interval $[0, 1]$. We assume that a high gradient occurs between the points $x = 1 - \delta$ and $x = 1$.

Let $q$ be a positive number. The problem is to determine the exponent $p$ of the exponential $e^{p(x-1)}$ such that the value of $e^{p(x-1)}$ at the point $x = 1 - \delta$ is $10^{-q}$, increasing from this value up to the point $x = 1$ where its value will be unity. Thus

$$e^{-p\delta} = 10^{-q}, \tag{17}$$

i.e.

$$p = -\frac{\ln(10^{-q})}{\delta} \tag{18}$$

and therefore

$$p = O\left(\frac{1}{\delta}\right). \tag{19}$$

Expression (19) determines the exponent $p$ of the exponential which simulates a boundary layer of width $\delta$.

Therefore we will have the following.

1. In directions orthogonal to streamlines,

$$p = O\left(\frac{1}{\delta}\right) = O\left(\sqrt{\left(\frac{v}{Dr}\right)}\right), \tag{20}$$

where $p$ is the exponent, $\delta$ is the width of the boundary layer and $r$ is the distance from the source point or the distance along the tangential boundary.

2. In streamline directions,

$$p = O\left(\frac{1}{\delta}\right) = O\left(\frac{v}{D}\right). \tag{21}$$

## 4. STRUCTURED MESH GENERATION

In this section we explain how to build a structured mesh for which the edges of the elements are in the high-gradient directions of the solution.

We know that at an interior or boundary layer a high variation in the solution can appear in the directions of streamlines and orthogonal to them. Therefore, to build a structured mesh, it is adequate to take the flow lines and their orthogonals as mesh lines. In Reference 14 the author proposes a simple procedure to generate this grid. Let us look at this procedure.

### *4.1. Construction of streamlines and their orthogonals*

1. The flow lines are built by integration from the inflow boundary $\Gamma_-$ of the differential equation

$$\frac{dy}{dx} = \frac{v_y}{v_x}. \tag{22}$$

2. The lines orthogonal to streamlines are built by integration of the differential equation

$$\frac{dy}{dx} = -\frac{v_x}{v_y} \tag{23}$$

from the boundary $\Gamma_0$.

Finite differences are used for numerical integration.

Figure 1 shows a structured mesh built from the streamlines and their orthogonals.

### *4.2. Geometrical mapping*

Let $\Omega^i$ be an element of the structured mesh and let $\tilde{\Omega}^i$ be a master element defined as $\tilde{\Omega}^i = [-1, 1] \times [-1, 1]$. Let $m$ be the total number of points of interpolation nodes of $\Omega^i$ and $\tilde{\Omega}^i$. We consider the mapping $\tau_i$: $\tilde{\Omega} \to \Omega^i$ defined by

$$x = \sum_{i=1}^{m} x_i \tilde{N}_i(\xi, \eta), \tag{24}$$

$$y = \sum_{i=1}^{m} y_i \tilde{N}_i(\xi, \eta), \tag{25}$$

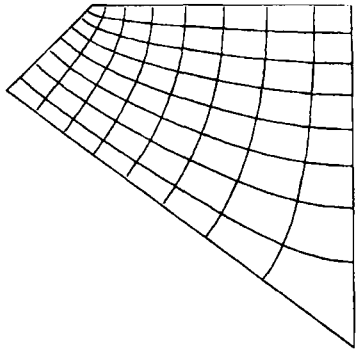

Figure 1. Structured mesh

where $\{\bar{N}_i(\xi, \eta)\}_{i=1}^{m}$ are the Lagrange interpolant polynomials for the geometry.

For each element $\Omega^i$ this bijective mapping generates a local grid of curved co-ordinates from the lines $\zeta = \text{const.}$ and $\eta = \text{const.}$ The high gradients of the function will occur along these lines. The exponential changes in an interior or boundary layer will occur in these directions, because the elements are generated from the streamlines and their orthogonals.

In the following section we define the basis of the elements placed in the boundary layer from the master element $\tilde{\Omega}^i$.

*Remark*

It is possible to make up an unstructured grid by proceeding as follows.

1. *In the zone where the boundary layer is located.* We copy the boundary, offsetting it towards the interior following the normal direction. From control points in the boundary translated in the normal direction, the boundary layer elements are built.
2. *In the external zone.* We proceed by generating an unstructured mesh geometrically compatible with the previous grid.

Figure 2 shows a mesh generated by means of this procedure.

## 5. DEFINITION OF THE SPACE OF APPROXIMATION $X_h$

In the previous section an explanation of how to build a structured mesh by splitting the domain into quadrangular elements has been given. In the zone of the boundary layer there are some elements whose edges are in the direction of high variation in the solution.

The aim of this section is to define the space of approximation $\tilde{X}_h$ in order to obtain a good representation of the boundary layer. This involves

(i) defining the space of approximation of the elements placed in the boundary layer by adding to the polynomial bases exponential functions able to represent the local behaviour of the solution

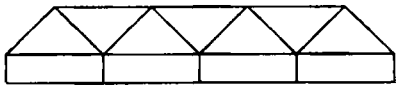

Figure 2. Unstructured mesh

(ii) giving coupling conditions between these elements and the polynomial standard elements placed outside the boundary layer
(iii) setting up a method in order to compute the order of exponential functions introduced in the new bases.

To define the basis functions, we use the following idea. For convection-dominated flows, i.e. for flows with large Reynolds number, we would like to have basis functions which act like solutions of the convection–diffusion equation; that is, we want to be able to represent narrow Gaussians which spread slowly as one goes downstream. In this sense we will define in this section the polynomial–exponential elements.

### *5.1. Polynomial–exponential elements*

We define the elements situated in the boundary layer by considering a master element $\tilde{\Omega}$ of co-ordinates $(\zeta, \eta)$.

*5.1.1. Unidirectional Element.* Let

$$\{L_i(z)\}_{i=0}^{N} \tag{26}$$

be a polynomial basis and

$$\{e^{j(z-1)}\}_{j\in J} \tag{27}$$

be a family of exponentials, where $J$ is a finite set of positive indices. In the direction $\eta$ we take the basis

$$\{e^{j(\eta-1)}\}_{j\in J} \bigcup \{L_i(\eta)\}_{i=0}^{N}, \tag{28}$$

with $\eta \in [-1, 1]$. In the direction $\zeta$ we take the basis

$$\{L_i(\zeta)\}_{i=0}^{N}, \tag{29}$$

with $\zeta \in [-1, 1]$.

The reference element $\tilde{\Omega}$ is defined as follows.

1. The tensorial product of both bases is taken as the interpolation basis in the square reference element. $PE1(\tilde{\Omega}_1)$ denotes the space of functions generated by the tensorial product, i.e.

$$PE1(\tilde{\Omega}_1) = \left\langle \{e^{j(\eta-1)}\}_{j\in J} \bigcup \{L_i(\eta)\}_{i=0}^{N} \right\rangle \otimes \langle \{L_i(\zeta)\}_{i=0}^{N} \rangle. \tag{30}$$

2. The interpolation nodes are the Cartesian products of the interpolation nodes in each direction. They are chosen according to the interpolation points of the polynomial basis. In this way it is easier to couple them with polynomial standard elements.

This element is able to represent an exponential behaviour in one direction in $\tilde{\Omega}$. We know that the mapping $\tau_i$: $\tilde{\Omega} \to \Omega^i$ generates a local grid of curved co-ordinates $(s, t)$, where the lines $\zeta = \text{const.}$ and $\eta = \text{const.}$ coincide with the streamlines and their orthogonals respectively. Therefore the exponential behaviour in one direction at element $\tilde{\Omega}$ will transfer to element $\Omega^i$ in the streamline directions or their orthogonals.

*5.1.2. Polynomial–exponential element in both directions.* The above families of exponentials and polynomials have been considered. In the direction $\eta$ the basis

$$\{e^{i(\eta-1)}\}_{i\in J} \bigcup \{L_i(\eta)\}_{i=0}^{N} \tag{31}$$

is taken, with $\eta \in [-1, 1]$. In the direction $\zeta$ the basis

$$\{L_j(\zeta)\}_{j=0}^{M} \bigcup \{e^{j(\zeta-1)}\}_{j\in J} \tag{32}$$

is taken, with $\zeta \in [-1, 1]$.

The reference element is defined as follows.

1. The tensorial product of both bases is taken as the interpolation basis in the square reference element. $PE2(\tilde{\Omega}_2)$ denotes the space of functions generated by the tensorial product, i.e.

$$PE2(\tilde{\Omega}_2) = \left\langle \{e^{i(\eta-1)}\}_{i\in J} \bigcup \{L_i(\eta)\}_{i=0}^{N} \right\rangle \otimes \left\langle \{L_j(\zeta)\}_{i=0}^{M} \bigcup \{e^{j(\zeta-1)}\}_{j\in J} \right\rangle. \tag{33}$$

2. The interpolation nodes are the Cartesian products of the interpolation nodes in each direction. They are chosen according to the interpolation points of the polynomial basis.

This element is able to represent exponential functions in both directions in $\tilde{\Omega}$ and thus in $\Omega^i$.

*5.2. Study of the coupling conditions between elements*

Over any oriented mesh there are polynomial–exponential elements and standard elements (finite or spectral elements). We are interested in the conditions of coupling between elements.

*5.2.1. Coupling of polynomial–exponential boundaries.* When boundary layer elements are adjoining, they must be coupled over the polynomial–exponential boundaries. It can be proved that if the order of exponentials is the same, then continuity between these types of boundaries exists.

The width of the boundary layer can change along the domain. Therefore the order of exponentials varies for two adjacent elements. This fact can be represented by using a non-conforming formulation. Among other formulations the pointwise matching technique has been chosen because of its simplicity.[4,15] In this formulation the same value of the function at the nodes of the boundary inter-elements is imposed.

Let $\Gamma^{ij}$ be the common polynomial–exponential boundary for two adjacent elements $\Omega^i$ and $\Omega^j$ and let $n_k$ be the nodes of this boundary, with $k = 1, \ldots, N$. Let $v^i$ and $v^j$ be the solutions in the elements $\Omega^i$ and $\Omega^j$ respectively.

The non-conforming coupling condition will be

$$v^i(n_k) = v^j(n_k), \quad k = 1, \ldots, N. \tag{34}$$

*5.2.2. Coupling of polynomial boundaries.* When two polynomial–exponential elements are adjacent in the polynomial boundary, they must be coupled. In the same way, when two standard elements are adjacent, their boundaries must also be coupled.

Three possibilities exist in order to couple these boundaries. The choice of one or another depends on factors such as the smoothness of the solution outside the boundary layer, the simplicity of the implementation and the size of the discrete problem.

1. *Coupling with the same polynomial degree.* Considering that the restrictions of the functions at the common boundary are polynomials of degree $N$, by forcing them to coincide in the $N+1$ points of the border, they must therefore coincide in the whole border.

2. *Coupling with different polynomial degrees.* The polynomial order in each element can vary; however, continuity can be maintained. In this case the following condition must be imposed: the value of the function along the common boundary is determined by the finest grid.[10]
3. *Non-conforming coupling.* In this case a pointwise matching technique or an integral matching technique (mortar elements) must be used.[2–4]

*Remark*

It is well known that the pointwise matching approach to non-conforming elements can be problematic.[2–4,16]

*5.2.3. Coupling of a polynomial boundary with a polynomial–exponential boundary.* This coupling is given between polynomial–exponential elements and polynomial elements.

Suppose that the restriction over the polynomial–exponential boundary is a polynomial of degree $N$ and one exponential. Under these conditions it is possible to carry out a conforming coupling between elements with the following restrictions.

1. The degree of the polynomial of the polynomial boundary must be less than or equal to $N$.
2. The function solution over the common boundary is determined by its values at the $N+2$ points of the finest grid.

*Summary*

From the above the coupling condition can be summarized.

*The value of the function along the boundary between two adjacent elements is determined by its values at the points of the finest grid.*

This condition will be denoted by CC (coupling condition) and can be written as follows.

Let $M_i$ and $M_j$ be two grids over the common boundary $\Gamma^{ij}$ of elements $\Omega^i$ and $\Omega^j$. Let us assume that $M_i$ is coarser than $M_j$. For all $x \in M_j$,

$$v^i|_{\Gamma^{ij}}(x) = v^j|_{\Gamma^{ij}}(x), \tag{35}$$

where $v^i|_{\Gamma^{ij}}(x)$ is the restriction at the boundary of the solution on element $\Omega^i$ and $v^j|_{\Gamma^{ij}}(x)$ is the restriction on element $\Omega^j$.

According to the type of boundary, the previous condition causes continuity or non-continuity of the function.

*5.3. Definition of the space of approximation*

Let us consider a structured mesh on the domain $\Omega$ so that

$$\Omega = \left(\bigcup_{i=1}^{N} \Omega_s^i\right) \bigcup \left(\bigcup_{j=1}^{M} \Omega_1^j\right), \tag{36}$$

where $\Omega_s^i$ denotes a standard element located outside the zone of the boundary layer and $\Omega_1^j$ denotes an element situated inside the boundary layer. Let $P_K(\Omega^i)$ denote the space of polynomials of degree $\leqslant K$.

The space of approximation is defined as

$$\tilde{X}_h = \{v \in L^2(\Omega)/v|_{\Omega_s^i} \in P_K(\Omega_s^i); (v \circ \tau^i)|_{\tilde{\Omega}} \in (PE1(\tilde{\Omega}_1) \quad \text{or} \quad PE2(\tilde{\Omega}_2)); (v(\Gamma^{ij}) \text{ satisfies the coupling condition and the boundary conditions})\}. \tag{37}$$

*5.4. Numerical study of the choice of the order of exponentials*

One of the most important aspects of the method formulated is the adequate choice of the number and order of exponentials in the bases of $\tilde{\Omega}$. The efficiency of the method is due to the property of the exponential functions that enables them to simulate a very strong variation using few exponentials and with small error.

*5.4.1. Approximation error of high gradients in a basis of exponential functions.* Let us carry out a study of the previous subjects. We will assume that the zone of the boundary or interior layer is simulated by exponentials whose order can vary in the interval $[n_i, n_f]$, with $n_i$ and $n_f$ natural numbers. Our aim is to establish a basis of exponential functions which correctly represent the exponential whose exponents belong to the interval $[n_i, n_f]$.

*Approximation error in a basis $\mathscr{B}$*

*Definition 1*

Let

$$\mathscr{B} = \{e^{a_i(z-1)}\}_{i \in I} \tag{38}$$

be an exponential basis, where $I$ is a finite set of indices, and let $e^{n(z-1)}$ be a known exponential, with $n \in [n_i, n_f]$ and $n_i$ and $n_f$ natural numbers. We define the $L^2$ error of approximation of the exponential $e^{n(z-1)}$ in this basis by

$$E_n = \left\| e^{n(z-1)} - \sum_{i=1}^{N} c_i e^{a_i(z-1)} \right\|_{L^2}, \tag{39}$$

where $c_i$ are the coefficients of the projection of $e^{n(z-1)}$ over the space generated by $\mathscr{B}$.

*Definition 2*

We define the accumulated error by

$$E_{ac} = \sum_{n=n_i}^{n=n_f} E_n, \tag{40}$$

with $n_i$ and $n_f$ natural numbers.

This error is obtained by the addition of the approximation error in the basis $\mathscr{B}$ of the exponentials whose orders are $n \in [n_i, n_f]$, with $n$ an integer number. It is a measure of the accuracy of the representation of the previous exponential functions in the basis $\mathscr{B}$. It can be proved that the approximation error of the derivative of $e^{n(z-1)}$ is $n$ times the $L^2$ error of the function $e^{n(z-1)}$, so that the $H^1$ error of $e^{n(z-1)}$ in the basis $\mathscr{B}$ is $(n+1)E_n$.

Suppose that the values $n_i$ and $n_f$ represent the lower and upper exponents of an interval whose range contains the exponents of the exponential functions simulating the high gradients. Suppose that we choose $[n_i, n_f]$ and we formulate the problem of determining the exponents of the basis $\mathscr{B}$ such that the accumulated error is minimum.

Once the number of exponentials in the basis $\mathscr{B}$ has been fixed, the solution of this problem provides the exponents of the exponentials that minimize the approximation error for the exponentials whose exponents are within the interval $[n_i, n_f]$. Owing to the relationship between the $L^2$ and $H^1$ errors, the exponents minimizing the $L^2$ error also minimize the $H^1$ error.

Table I. Range of variation in error

| Exponential | $L^2$ error | $H^1$ error |
|---|---|---|
| 10 | 0·000689672 | 0·00768923 |
| 11 | 0·000332962 | 0·00405746 |
| 12 | 0·000142812 | 0·00188986 |
| 13 | $4{\cdot}88442 \times 10^{-5}$ | 0·000698597 |
| 20 | $5{\cdot}79728 \times 10^{-5}$ | 0·00124314 |
| 30 | $6{\cdot}23552 \times 10^{-5}$ | 0·00201288 |
| 40 | $2{\cdot}07978 \times 10^{-5}$ | 0·000914871 |
| 50 | $3{\cdot}40249 \times 10^{-6}$ | 0·000199793 |
| 60 | $4{\cdot}47781 \times 10^{-8}$ | $5{\cdot}81744 \times 10^{-6}$ |
| 70 | $2{\cdot}87135 \times 10^{-7}$ | $1{\cdot}60846 \times 10^{-5}$ |
| 80 | $4{\cdot}3369 \times 10^{-7}$ | $3{\cdot}23897 \times 10^{-5}$ |
| 90 | $1{\cdot}34776 \times 10^{-7}$ | $1{\cdot}24532 \times 10^{-5}$ |
| 100 | $3{\cdot}48545 \times 10^{-8}$ | $2{\cdot}57108 \times 10^{-6}$ |
| 110 | $8{\cdot}06447 \times 10^{-7}$ | $8{\cdot}03488 \times 10^{-5}$ |
| 120 | $2{\cdot}87574 \times 10^{-6}$ | 0·000322353 |
| 130 | $6{\cdot}41325 \times 10^{-6}$ | 0·000789929 |
| 140 | $1{\cdot}14005 \times 10^{-5}$ | 0·00152531 |
| 150 | $1{\cdot}77023 \times 10^{-5}$ | 0·00255267 |
| 160 | $2{\cdot}5123 \times 10^{-5}$ | 0·0038812 |
| 170 | $3{\cdot}34454 \times 10^{-5}$ | 0·00550854 |
| 180 | $4{\cdot}24547 \times 10^{-5}$ | 0·00742398 |
| 190 | $5{\cdot}19524 \times 10^{-5}$ | 0·00961115 |

*Example*

Let us consider $[n_i, n_f] = [10, 200]$. Choose three functions in the basis and pose the following problem.

1. Compute the exponents $a_1$, $a_2$ and $a_3$ minimizing the error of representation in the basis of the exponentials whose exponents are in [10, 200].
2. Compute the accumulated error.
3. Compute the error for each exponential.

For the computation of exponents $a_i$ under the condition that the error $E_{ac}(a_i)$ is minimum, an algorithm of gradient, together with the bisection method for the determination of step length, has been used. The results obtained for the three exponentials are as follows.

1. The exponents which minimize the accumulated error are 15·0071, 62·9203 and 97·3525.
2. The accumulated error is $4{\cdot}8 \times 10^{-3}$.
3. The $L^2$ and $H^1$ errors are given in Table I.

Therefore it is possible to represent a range of variation in exponentials with small error and using few exponentials.

*5.4.2. How to compute the exponentials to add to boundary layer elements.* We know that in local co-ordinates $(s, t)$ the relationship between the width of the boundary layer and the exponent $p$ of the exponential that simulates this boundary is

$$p = O\left(\frac{1}{\delta}\right). \tag{41}$$

Therefore we will have the following.

1. In directions orthogonal to streamlines,

$$p = O\left(\frac{1}{\delta}\right) = O\left(\sqrt{\left(\frac{v}{Dr}\right)}\right), \tag{42}$$

where $p$ is the exponent, $\delta$ is the width of the boundary layer and $r$ is the distance from the source point or the distance along the tangential boundary.

2. In streamline directions,

$$p = O\left(\frac{1}{\delta}\right) = O\left(\frac{v}{D}\right). \tag{43}$$

The above relationship supplies the interval of variation in the exponents in the $s$-direction and $t$-direction in element $\Omega^i$.

Let us look at the relationship between the intervals of the exponents in element $\Omega^i$ and the reference element $\tilde{\Omega}$. We will consider a linear approximation of element $\Omega^i$ referred to a curved co-ordinate system $(s, t)$. In this system the linear approximation will be $\Omega^i = [0, a] \times [0, b]$.

Suppose that in the $s$-direction there is an exponential $e^{p(s-a)}$ with exponent $p$. To compute the exponent for the basis of $\tilde{\Omega}$, we consider the linear transformation $T$: $\tilde{\Omega} \to [0, a] \times [0, b]$ defined by

$$s = \frac{a}{2}(\zeta + 1), \tag{44}$$

$$t = \frac{b}{2}(\eta + 1). \tag{45}$$

Thus we will have

$$e^{p(s-a)} = e^{p[(a/2)(\zeta+1)-a]} = e^{p[(a/2)(\zeta-1)]}; \tag{46}$$

that is, if the exponent of the exponential in element $\Omega^i$ is $p$, then $p(L/2)$ is the exponent in $\tilde{\Omega}$, where $L$ is the length in the $s$-direction for element $\Omega^i$.

Once we know the interval of the exponents in $\tilde{\Omega}$, we must determine the basis of the exponential to add to $\tilde{\Omega}$. To this end we fix the number of exponentials in the basis. Then, applying the minimization algorithm for the accumulated error considering the interval calculated above, we will have the exponential to add to $\tilde{\Omega}$.

## 6. SHAPE FUNCTIONS AND QUADRATURE FORMULAE

### *6.1. Shape functions*

To obtain the nodal approximation, the expression of the shape functions for the master element $\tilde{\Omega}$ must be calculated.

Let $\phi_i(\zeta, \eta)$ be the functions resulting from the tensorial products of the bases in both directions. We consider the non-nodal approximation

$$\Phi(\zeta, \eta) = \sum_{i=1}^{n} a_i \phi_i(\zeta, \eta), \tag{47}$$

where $a_i$ are the approximation coefficients and $n$ is the total number of functions in the basis.

Let $N_i(\zeta, \eta)$ be the shape functions to be calculated. The nodal approximation will be

$$\Phi(\zeta, \eta) = \sum_{i=1}^{n} \Phi(\zeta, \eta)_i N_i(\zeta, \eta). \tag{48}$$

Taking into account the uniqueness of the expression $\Phi(\zeta, \eta)$, we can obtain

$$[N_i(\zeta, \eta)]^{\mathrm{T}} = [\phi_i(\zeta, \eta)]^{\mathrm{T}} [\phi_i(\zeta, \eta)_j]^{-1}. \tag{49}$$

### 6.2. *Quadrature formulae*

It is well known that when an exponential function is integrated by a polynomial quadrature formula, the quadrature errors increase by a factor of $a^{n+1}/(n+1)!$, where $a$ is the order of the exponential and $n$ is the order of the polynomial approximation. Therefore the use of Gauss quadrature formulae for polynomials is not suitable for the integration of polynomial–exponential functions because of the large number of points of integration necessary.

To integrate products of functions of the basis

$$\{e^{i(z-1)}\}_{i \in I} \bigcup \{L_i(z)\}_{i=0}^{N} \tag{50}$$

and its derivatives, we must compute the weights and points of a quadrature formula. Let $p$ be the number of functions to be integrated and let $f(z)$ be a linear combination of these $p$ functions:

$$f(z) = \sum_{i=1}^{p} a_i f_i(z). \tag{51}$$

There are two possibilities.

If the $p$ points of the quadrature are chosen using the equation

$$\int_{-1}^{1} f(z) = \sum_{r=1}^{p} w_r f(z_r), \tag{52}$$

we obtain a linear system with $p$ equations and $p$ unknowns,

$$\int_{-1}^{1} f_i(z) = \sum_{r=1}^{p} w_r f_i(z_r), \tag{53}$$

with $i = 1, 2, \ldots, p$, whose resolution supplies the weights $\{w_r\}_{r=1}^{p}$.

The other possibility is to economize the number of points and weights by considering the points and weights as free. Taking an even number of functions, $p$, a non-linear system with $p$ equations and $p$ unknowns $\{w_r, zr\}_{r=1}^{p/2}$ can be obtained:

$$\int_{-1}^{1} f_i(z) = \sum_{r=1}^{p/2} w_r f_i(z_r), \tag{54}$$

with $i = 1, 2, \ldots, p$. To solve this non-linear system, a globally convergent method must be used.[17]

Therefore we need $p$ weights to integrate $p$ functions in the case where we work with $p$ fixed points, and $p/2$ weights and $p/2$ points in the opposite non-linear case.

## 7. ALGORITHM STEPS AND NUMERICAL EVALUATION OF THE ALGORITHM

The proposed method consists of the discretization of the Galerkin formulation of the problem over a structured mesh made up of both standard (finite or spectral elements) and polynomial–exponential elements. In this section the steps of the algorithm are summarized. Moreover, numerical evaluation of the properties of the method will be carried out by means of a set of test problems.

### *7.1. Inputs and algorithm steps*

The implementation of the method does not differ from the standard method with regard to the construction procedure of the matrix of the discrete problem.

The main differences are as follows.

1. A structured mesh which locates the boundary layer zone can be built from the information concerning the boundary layer.
2. Since exponential functions must be added to some elements, the shape functions of such elements and the quadrature formulae are specific to the method.

*Inputs*

The algorithm needs to be aware of three inputs.

1. *Input 1.* The position of the boundary layer or equivalently the placement of control points on the domain to locate the boundary layer.
2. *Input 2.* Estimation of the width of the boundary layer.
3. *Input 3.* Knowledge of the field of velocities.

*Algorithm steps*

*Step 1* (using Inputs 1 and 3)

(a) Starting from control points on $\Gamma_-$, compute the streamlines by solving

$$\frac{dy}{dx} = \frac{v_y}{v_x}. \tag{55}$$

(b) Starting from control points on $\Gamma_0$, compute the lines orthogonal to streamlines by solving

$$\frac{dy}{dx} = -\frac{v_x}{v_y}. \tag{56}$$

(c) Classify the elements as (i) standard (finite or spectral), (ii) polynomial–exponential in one direction (*PE*1) or (iii) polynomial–exponential in two directions (*PE*2) and determine the degrees of polynomial interpolation.

*Step 2* (using Input 2). Compute the order of exponentials to include *PE*1 and *PE*2 by calculating the following two items:

(a) the interval of variation in the exponents for the exponential functions, taking into account that the relationship between the exponents and the width of the boundary layer is, (i) in directions orthogonal to streamlines,

$$p = O\left(\frac{1}{\delta}\right) = O\left(\sqrt{\left(\frac{v}{Dr}\right)}\right), \tag{57}$$

$p$ being the exponent, $\delta$ the width of the boundary layer and $r$ the distance to the source point, and (ii) in streamline directions,

$$p = O\left(\frac{1}{\delta}\right) = O\left(\frac{v}{D}\right) \tag{58}$$

(b) the basis of exponentials minimizing the accumulated error (see the algorithm in the section referring to exponentials).

*Step 3.* Calculate the shape functions of $PE1$ and $PE2$ elements by solving

$$[N_i(\zeta, \eta)]^{\mathrm{T}} = [\phi_i(\zeta, \eta)]^{\mathrm{T}}[\phi_i(\zeta, \eta)_j]^{-1}. \tag{59}$$

(Here $\phi_i(\zeta, \eta)$ are the functions resulting from the tensorial products of the bases in both directions and $N_i(\zeta, \eta)$ are the shape functions.)

*Step 4.* Compute the weights and quadrature points for $PE1$ and $PE2$ elements by solving

$$\int_{-1}^{1} f_i(z) = \sum_{r=1}^{p/2} w_r f_i(z_r), \tag{60}$$

with $i = 1, 2, \ldots, p$.

*Step 5.* Calculate the bilinear form $a(\phi_h, \Psi_h)$ and the linear form $l(f)$ over each element and assemble the matrix, taking into account the coupling condition CC between elements. (The coupling condition CC is as follows. Let $M_i$ and $M_j$ be two grids over the common boundary $\Gamma^{ij}$ of elements $\Omega^i$ and $\Omega^j$. Let us assume that $M_i$ is coarser than $M_j$. For all $x \in M_j$,

$$v^i|_{\Gamma^{ij}}(x) = v^j|_{\Gamma^{ij}}(x), \tag{61}$$

where $v^i|_{\Gamma^{ij}}(x)$ is the restriction at the boundary of the solution on element $\Omega^i$ and $v^j|_{\Gamma^{ij}}(x)$ is the restriction on element $\Omega^j$.)

### 7.2. *Test problems and evaluation of the algorithm*

We are interested to know the behaviour of the method as regards

(i) the error of approximation
(ii) the computational cost
(iii) the behaviour of the method when $D$ decreases.

We will consider the following test problems in order to study these three points.

*7.2.1. Problem 1: Interior layer due to a Dirac delta source term.* The convection–diffusion equation has been considered with a Dirac delta source term, constant diffusion $D$ and constant velocity $v$:

$$\begin{aligned} -D\Delta\phi + v\frac{\partial\phi}{\partial x} &= k\delta(x-x_0)\delta(y-y_0), \quad (x,y) \in (0,2)\times(0,2), \\ \phi &= 0, \quad x=0, y=2, y=0, \\ \frac{\partial\phi}{\partial n} &= 0, \quad x=2. \end{aligned} \tag{62}$$

We have considered two implementations, taking one exponential in the streamline direction and two or three exponentials in orthogonal directions.

*Data*

The implementation data of the problem are the following:

(i) domain $[0, 2]\times[0, 2]$
(ii) $\mathbf{v} = (3{\cdot}75\times10^{-3}, 0)$
(iii) escape point localized at (1, 1) and with volume escape $k = 8{\cdot}33\times10^{-6}$
(iv) $D = 0{\cdot}15\times10^{-4}$.

The Peclet and Reynolds numbers for this problem are $Pe = 500$ and $Re = 497$.

*Localization of the interior layer and behaviour*

An interior source point generates an interior layer in a nearly circular region around this point in the streamline direction, its size being $O(D/v)$. Downstream from this point an internal layer develops along the streamline in the orthogonal direction, its width being $O(\sqrt{(rD/v)})$, where $r$ is the distance downstream from the source point.

*Algorithm steps*

*(a) Grid generation*

The streamlines and orthogonals are reduced to lines parallel to the co-ordinate axes. The grid shown in Figure 3 has been considered, elements 1 and 8 being of type $PE2$ and the remainder of type $PE1$.

*(b) Exponentials to add to the basis*

The order of exponentials in streamline directions is $O(v/D) = O(250)$ in the element of the mesh. Therefore in the reference element the exponent is $O(125)$. The interval of variation in the exponentials in directions orthogonal to streamlines, calculated from the width of the interior layer, is [15, 70]. Thus the interval to represent in the reference element is [7, 35]. However, the interval [5, 80] has been considered in order to compensate for proportionality factors.

*Bases for two exponentials.* Using the algorithm of minimization of the error, for exponentials 7 and 20 the accumulated error is $1{\cdot}3\times10^{-2}$. Therefore we consider a conforming mesh formed by two $PP2$ elements and six $PP1$ elements whose bases are

(i) $PE2$ element in direction $\zeta$: $L_0(\zeta), L_1(\zeta), e^{125(\zeta-1)}$

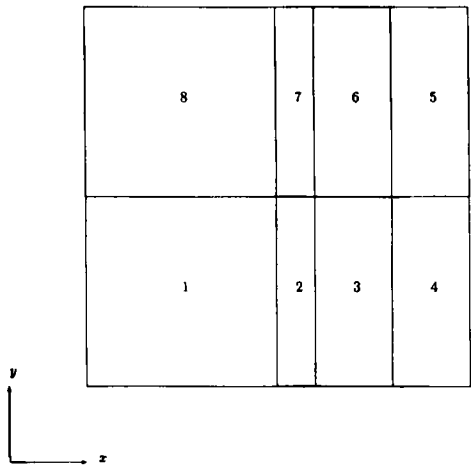


Figure 3. Scheme of polynomial–exponential elements

(ii) $PE2$ element in direction $\eta$: $L_0(\eta), L_1(\eta), L_2(\eta), e^{7(\eta-1)}, e^{20(\eta-1)}$
(iii) $PE1$ element in direction $\zeta$: $L_0(\zeta), L_1(\zeta), L_2(\zeta)$
(iv) $PE1$ element in direction $\eta$: $L_0(\eta), L_1(\eta), L_2(\eta), e^{7(\eta-1)}, e^{20(\eta-1)}$

where $L_i$ are Legendre polynomials. There are 81 nodes in the grid, 49 of which are interiors.

*Bases for three exponentials.* Using the algorithm of minimization of the error, for exponentials 7, 20 and 30 the accumulated error is $6{\cdot}8 \times 10^{-3}$. In this case a conforming mesh formed by two $PP2$ elements and six $PP1$ elements has been considered. In $\tilde{\Omega}$ the bases are

(i) $PE2$ element in direction $\zeta$: $L_0(\zeta), L_1(\zeta), e^{125(\zeta-1)}$
(ii) $PE2$ element in direction $\eta$: $L_0(\eta), L_1(\eta), e^{7(\eta-1)}, e^{20(\eta-1)}, e^{30(\eta-1)}$
(iii) $PE1$ element in direction $\zeta$: $L_0(\zeta), L_1(\zeta), L_2(\zeta)$
(iv) $PE1$ element in direction $\eta$: $L_0(\eta), L_1(\eta), e^{7(\eta-1)}, e^{20(\eta-1)}, e^{30(\eta-1)}$.

There are 81 nodes in the grid.

### *(c) Quadrature points*

Taking into account that the functions to be integrated are obtained as the products of the functions of the above basis in each direction and its derivatives, we require seven points in the $\eta$-direction and three points in the $\zeta$-direction for the $PP2$ element. For the $PP1$ element we require seven points in the $\eta$-direction and two points in the $\zeta$-direction. Therefore the total number of integration points for the mesh is 126.

### *Results*

Figures 4 and 5 show the solution in the case of two exponentials. Figures 6 and 7 show the solution in the case of three exponentials.

The oscillations in the neighbourhood of the source point in Figure 4 are due to the difficulty in representing a high gradient with an exponential of order 20. If a third exponential of order 30 is taken, the oscillations are removed.

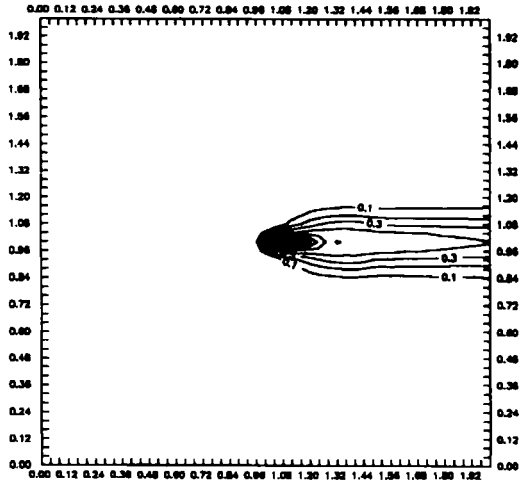


Figure 4. Solution with two exponentials

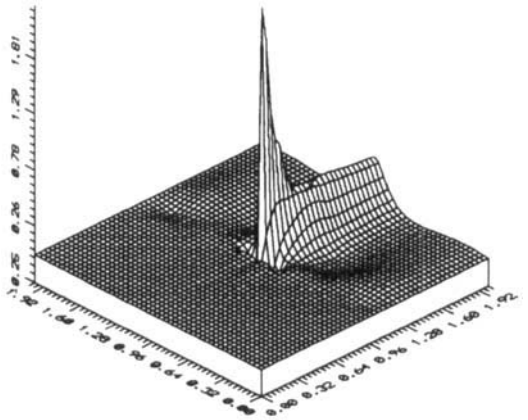

Figure 5. Solution with two exponentials

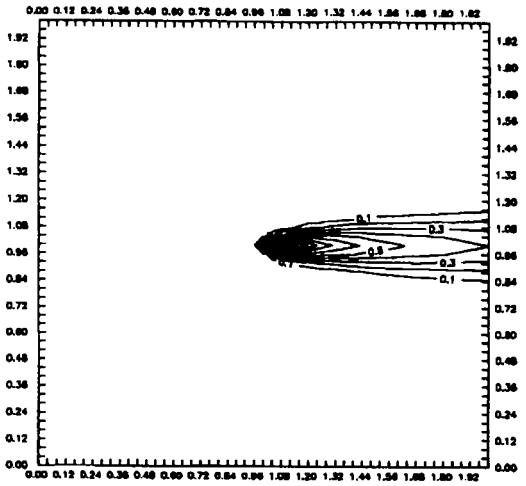


Figure 6. Solution with three exponentials

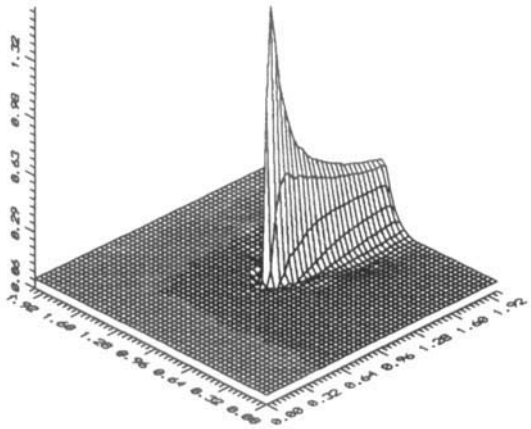

Figure 7. Solution with three exponentials

*Evaluation of the error*

For the evaluation of the error in the absence of analytical solutions, even for simple geometries, we have considered the following procedures.

(a) Let $\Phi$ be the actual solution of the problem. Thus

$$\Phi = \Phi_h + e_h, \tag{63}$$

where $\Phi_h$ is the numerical solution obtained and $e_h$ is the exact error. Substituting in the equation

$$\int_\Omega D\nabla\Phi\nabla\Psi + u\int_\Omega \frac{\partial\Phi}{\partial x}\Psi = k\int_\Omega \delta(x - x_0)(y - y_0)\Psi, \tag{64}$$

we obtain

$$\int_\Omega D\nabla e_h\nabla\Psi + u\int_\Omega \frac{\partial e_h}{\partial x}\Psi = -\int_\Omega D\nabla\Phi_h\nabla\Psi - u\int_\Omega \frac{\partial\Phi_h}{\partial x}\Psi + k\int_\Omega \delta(x - x_0)(y - y_0)\Psi. \tag{65}$$

This is a convection–diffusion equation in that the independent term depends on the numerical solution $\Phi_h$ obtained. To solve this equation, we have considered a triangular mesh formed by linear finite elements, which is adapted to the problem from the information obtained from the distribution of the residue. The numerical value of $e_h$ is taken as the actual value of the error and in particular the $L^2$-norm of $e_h$ has been considered.

*Remark.* The fundamental solution for equation (62) on the whole plane is a Bessel function with a logarithmic singularity at the source point.[18] The finite element method (FEM) and the algorithm developed cannot represent this fact. It is possible to establish that the value which is assigned to the source point by each method depends on the trial functions and it is different at this point, although it is coincidental over other points of the grid. Therefore, if we remove from the domain a small neighbourhood around the source point, the distortions due to the former phenomenon are reduced.

(b) The second procedure to evaluate the error lies in comparing the numerical solution with other numerical solutions computed by the Galerkin method or the streamline upwind Petrov–Galerkin (SUPG) method. More exactly, we take a non-uniform mesh of triangles; we consider the numerical solutions of the equation in that grid for the FEM–Galerkin and SUPG methods and we denote them by

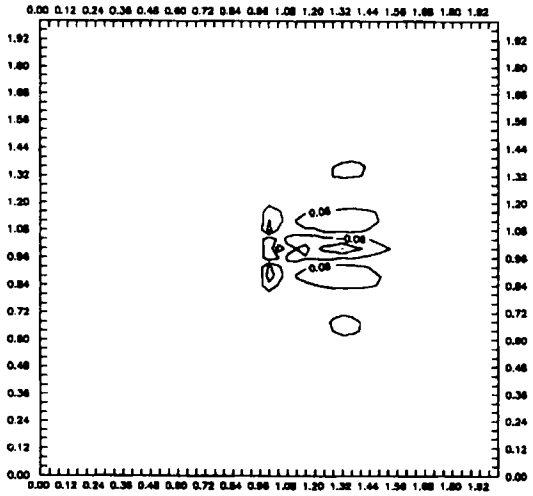

Figure 8. Distribution of error for two exponentials

$\Phi_G$ and $\Phi_{PG}$ respectively. The solution furnished by the algorithm developed in this work is denoted by $\Phi_{EEM}$. This solution is interpolated over the triangular mesh. We compute the values

$$\|\Phi_{PG} - \Phi_{EEM}\|_{L^2}, \tag{66}$$

$$\frac{\|\Phi_G - \Phi_{EEM}\|_{L^2}}{\|\Phi_G\|_{L^2}}, \quad \frac{\|\Phi_{PG} - \Phi_{EEM}\|_{L^2}}{\|\Phi_{PG}\|_{L^2}}, \quad \frac{\|\Phi_{PG} - \Phi_G\|_{L^2}}{\|\Phi_G\|_{L^2}}, \quad \frac{\|\Phi_G - \Phi_{PG}\|_{L^2}}{\|\Phi_G\|_{L^2}}, \tag{67}$$

which measure respectively the absolute error and the relative error between the solutions which are compared.

*Computation of the $L^2$ error*

The error computed for the two strategies is as follows.

(a) We resolve equation (65) over a non-uniform grid with 488 nodes (944 linear triangular elements) by removing from the domain a square of side 0·1 centred at the source point:

(i) $\|e_h\|_{L^2} = 1{\cdot}5640 \times 10^{-3}$ for the implementation with two exponentials
(ii) $\|e_h\|_{L^2} = 5{\cdot}0963 \times 10^{-4}$ for the implementation with three exponentials.

Figures 8 and 9 show the distribution of error in both cases.

(b) For the second procedure we have considered the solutions supplied by Galerkin and Petrov–Galerkin methods over the former grid. Figure 10 shows the Petrov–Galerkin solution.

The evaluation of the norms and their quotients has been carried out by working over the full domain without removing the neighbourhood around the escape point. The most important fact is that in the case of two exponentials (7 and 20) the error defined by

$$\frac{\|\Phi_{PG} - \Phi_{EEM}\|_{L^2}}{\|\Phi_{PG}\|_{L^2}} \tag{68}$$

is around 3·4%. By removing a small square around the source point, the evaluated error decreases. Working with three exponentials (7, 20 and 30) over the full domain, the error is 1·7% and this

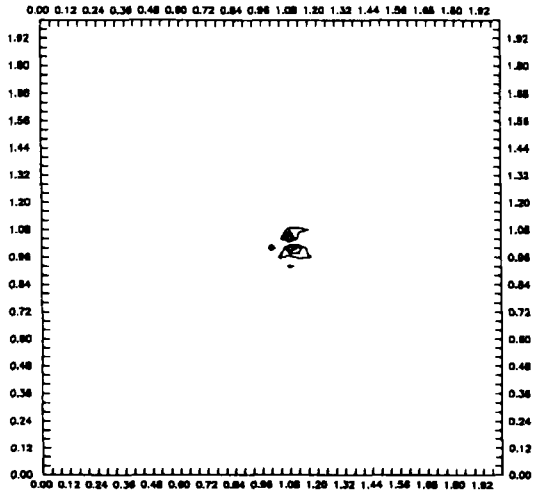

Figure 9. Distribution of error for three exponentials

decreases if we eliminate the square around the source point. In the same way, if the absolute error is computed,

$$\|\Phi_{PG} - \Phi_{EEM}\|_{L^2}, \tag{69}$$

we can verify in Tables II and III that it decreases when working with three exponentials. The results for both cases have been tabulated in these tables.

*Remark.* If we consider a vectorial field of velocities to determine the exponential order of exponential functions, we can take as value of the velocity in each element the average value considering the inflow and outflow velocities in the element.

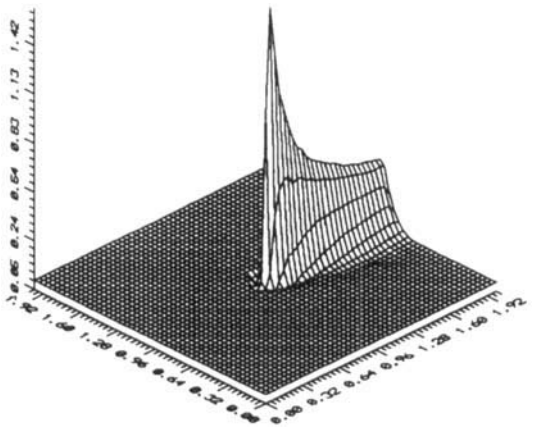

Figure 10. Petrov–Galerkin solution

Table II. $L^2$-norm for two exponentials

| Exponentials | 7, 20 |
|---|---|
| $\|\Phi_{EEM}\|_{L^2}$ | 0·0523121210607842 |
| $\|\Phi_{PG}\|_{L^2}$ | 0·0531518325217073 |
| $\|\Phi_{G}\|_{L^2}$ | 0·0543980240137801 |
| $\dfrac{\|\Phi_{PG} - \Phi_{EEM}\|_{L^2}}{\|\Phi_{PG}\|_{L^2}}$ | 0·034309263014138 |
| $\dfrac{\|\Phi_{G} - \Phi_{EEM}\|_{L^2}}{\|\Phi_{G}\|_{L^2}}$ | 0·0349285817264169 |
| $\dfrac{\|\Phi_{PG} - \Phi_{G}\|_{L^2}}{\|\Phi_{G}\|_{L^2}}$ | 0·00280232274699124 |
| $\dfrac{\|\Phi_{G} - \Phi_{PG}\|_{L^2}}{\|_{G}\|_{L^2}}$ | 0·00286802567010149 |
| $\|\Phi_{PG} - \Phi_{EEM}\|_{L^2}$ | $1{\cdot}8 \times 10^{-3}$ |

Table III. $L^2$-norm for three exponentials

| Exponentials | 7, 20, 30 |
|---|---|
| $1\|\Phi_{EEM}\|_{L^2}$ | 0·0481781023781807 |
| $1\|\Phi_{PG}\|_{L^2}$ | 0·0531518325217073 |
| $11\|\Phi_{G}\|_{L^2}$ | 0·0543980240137801 |
| $\dfrac{\|\Phi_{PG} - \Phi_{EEM}\|_{L^2}}{\|\Phi_{PG}\|_{L^2}}$ | 0·0171556674056386 |
| $\dfrac{\|\Phi_{G} - \Phi_{EEM}\|_{L^2}}{\|\Phi_{G}\|_{L^2}}$ | 0·0187092346747842 |
| $\dfrac{\|\Phi_{PG} - \Phi_{G}\|_{L^2}}{\|\Phi_{G}\|_{L^2}}$ | 0·00280232274699124 |
| $\dfrac{\|\Phi_{G} - \Phi_{PG}\|_{L^2}}{\|\Phi_{G}\|_{L^2}}$ | 0·00286802567010149 |
| $\|\Phi_{PG} - \Phi_{EEM}\|_{L^2}$ | $9{\cdot}12 \times 10^{-4}$ |

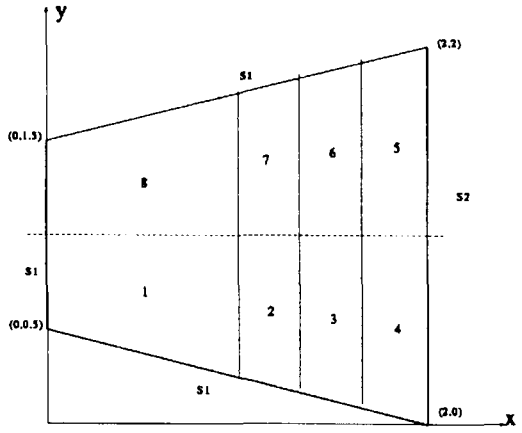


Figure 11. Scheme of polynomial–exponential elements

We have considered the following example:

$$\begin{aligned} -D\Delta\phi + \mathbf{v}(x,y)\nabla\phi &= k\delta(x-1)\delta(y-1), \qquad (x,y) \in \Omega, \\ \phi &= 0, \qquad (x,y) \in S_1, \\ \frac{\partial\phi}{\partial n} &= 0, \qquad (x,y) \in S_2, \end{aligned} \tag{70}$$

where $\Omega$ is the domain shown in Figure 11 and $S_1$ and $S_2$ are specified in this figure. We assume the following vectorial field of velocities $\mathbf{v} = (v_x, v_y)$:

$$v_x = v(r)\frac{2+x}{r}, \qquad v_y = v(r)\frac{y-1}{r}, \tag{71}$$

where

$$r = \sqrt{[(x+2)^2 + (y-1)^2]}, \qquad v(r) = \frac{0 \cdot 015}{r}. \tag{72}$$

This velocity field is equivalent to a radial flow with a source at point $(-2, 1)$. The mesh we have considered is shown in the same figure.

If we calculate the absolute values of the inflow and outflow velocities in each element, we obtain that the order of exponential functions in *PE*1 elements in streamline directions is $O(167)$. In *PE*2 elements in directions orthogonal to streamlines this order is between $O(13)$ and $O(10)$.

The solution of this example is shown in Figure 12.

*7.2.2. Problem 2: Boundary layer due to boundary conditions, with gradients orthogonal to streamline directions.* Let us consider the convection–diffusion equation (62) without the source term, with the same boundary conditions except for the upwind side. At the inflow boundary we take the symmetrization of the function $g(y) = e^{25(y-0.5)}$, which is denoted by $f(y)$.

$$\begin{aligned} -D\Delta\phi + v\frac{\partial\phi}{\partial x} &= 0, \quad (x,y) \in (0,1) \times (0,1), \\ \phi &= 0, \quad y = 1, y = 0, \\ \phi &= f(y), \quad x = 0, \\ \frac{\partial\phi}{\partial n} &= 0, \quad x = 1. \end{aligned} \tag{73}$$

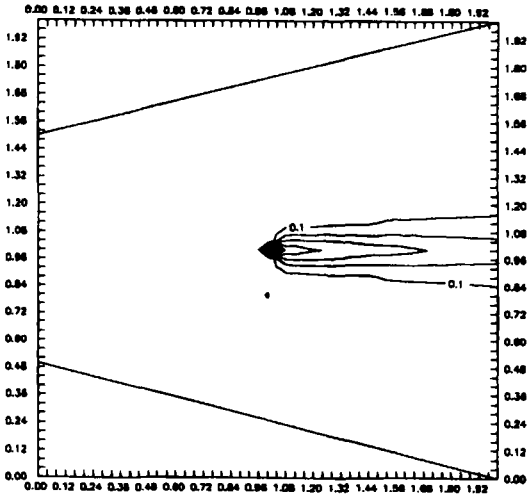


Figure 12. Solution for a vectorial velocity field

The velocity is $\mathbf{v} = (2{\cdot}6 \times 10^{-3}, 0)$ and the diffusion is $D = 0{\cdot}15 \times 10^{-4}$. The Peclet and Reynolds numbers are $Pe = 173$ and $Re = 172$.

The analytical solution of this problem is known:[10]

$$\phi(x, y) = 2e^{(v/2D)x} \sum_{n=1}^{\infty} \frac{\int_0^1 f(y) \sin(n\pi y)\, dy}{1 + c_n} F(n, x) \sin(n\pi y) \tag{74}$$

where

$$F(n, x) = e^{\sqrt{[n^2\pi^2 + (v/2D)^2]}x} + c_n e^{-\sqrt{[n^2\pi^2 + (v/2D)^2]}x}, \tag{75}$$

$$c_n = \frac{2v^2 + 4(Dn\pi)^2 + 2v\sqrt{[v^2 + 4(Dn\pi)^2]}}{4(Dn\pi)^2} e^{\sqrt{[4n^2 + \pi^2 + (v/2D)^2]}}. \tag{76}$$

The solution is symmetric with respect to the line $y = 0{\cdot}5$ owing to the characteristics of the boundary conditions and of the velocity field. Therefore, to solve problem (73), we have considered the domain $(0, 1) \times (0, 0{\cdot}5)$. On the boundary $y = 0{\cdot}5$ the values of the series have been considered. Then the problem to be solved is

$$\begin{aligned} -D\Delta\phi + v\frac{\partial\phi}{\partial x} &= 0, & (x, y) &\in (0, 1) \times (0, 0{\cdot}5), \\ \phi &= 0, & y &= 0, \\ \phi = g(y) &= e^{25(y-0{\cdot}5)}, & x &= 0, \\ \phi &= h(x), & y &= 0{\cdot}5, \\ \frac{\partial\phi}{\partial n} &= 0, & x &= 1, \end{aligned} \tag{77}$$

where $h(x)$ denotes the values of the series (74).

Problem (77) has a boundary layer with parabolic profile in $y = 0{\cdot}5$ and thickness $O(\sqrt{(DL/v)}) = 13$, where $L$ is the characteristic length. Therefore we consider the interval [5, 15] as the interval of variation in the exponents to be represented in $\tilde{\Omega}$.

We are interested in studying the $L^2$ and $H^1$ errors for conforming and non-conforming implementations. The bases and results are detailed in the following.

*(a) Two exponentials, Conforming mesh*

*Basis*

(i) In direction $x$: $L_0$, $L_1$, $L_2$.
(ii) In direction $y$: $L_0$, $L_1$, $L_2$, $e^{5\cdot1(y-1)}$, $e^{10\cdot13(y-1)}$.

*Errors*

(i) The $L^2$ error of the function is $6\cdot7134522025 \times 10^{-6}$.
(ii) The $L^2$ error of the derivatives is $3\cdot786206781061368 \times 10^{-4}$.
(iii) The $H^1$ error is $3\cdot85334130308 \times 10^{-4}$.

*(b) Three exponentials, Conforming mesh*

*Basis*

(i) In direction $x$: $L_0$, $L_1$, $L_2$.
(ii) In direction $y$: $L_0$, $L_1$, $L_2$, $e^{5\cdot1(y-1)}$, $e^{10\cdot13(y-1)}$, $e^{15\cdot35(y-1)}$.

*Errors*

(i) The $L^2$ error is $3\cdot235907714 \times 10^{-6}$.
(ii) The $L^2$ error of the derivatives is $1\cdot93144815337 \times 10^{-4}$.
(iii) The $H^1$ error is $1\cdot96380723051 \times 10^{-4}$.

*(c) Two exponentials, Non-conforming mesh*

*Basis*

(i) In direction $x$: $L_0$, $L_1$, $L_2$.
(ii) In direction $y$: $L_0$, $L_1$, $L_2$, $e^{15(y-1)}$, $e^{8(y-1)}$.
(iii) In direction $x$: $L_0$, $L_1$, $L_2$.
(iv) In direction $y$: $L_0$, $L_1$, $L_2$, $e^{8(y-1)}$, $e^{3(y-1)}$.

*Errors*

(i) The $L^2$ error is $1\cdot321395904674676 \times 10^{-6}$.
(ii) The $L^2$ error of the derivatives is $4\cdot969053032568501 \times 10^{-4}$.
(iii) The $H^1$ error is $4\cdot982266991615248 \times 10^{-4}$.

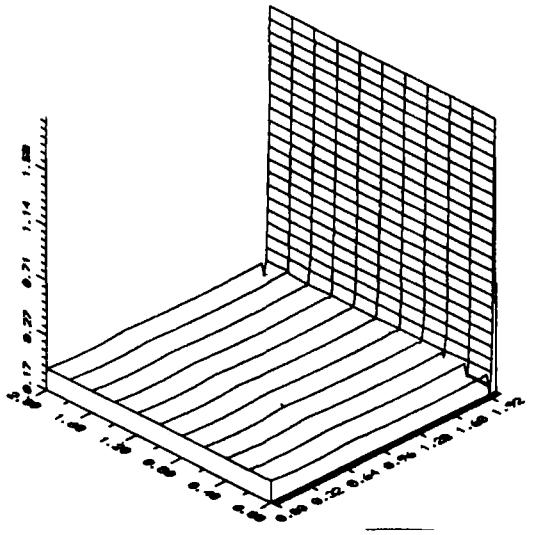

Figure 13. Boundary layer due to boundary conditions

*7.2.3. Problem 3: Boundary layer due to boundary conditions, with gradients in streamline directions.* Finally, the following problem has been considered:

$$\begin{aligned} -D\Delta\phi + v\frac{\partial\phi}{\partial x} &= 0, \quad (x,y) \in (0,1)\times(0,1), \\ \phi &= 0, \quad x = 0, y = 1, y = 0, \\ \phi &= 2, \quad x = 1. \end{aligned} \tag{78}$$

Figure 13 shows the solution for $D = 1 \times 10^{-6}$ and $v = 1{\cdot}0$. The Peclet and Reynolds numbers are $Pe = 10^6$ and $Re = 66{,}225$.

In this problem the boundary layer is located on the boundary $x = 1$ in the streamline direction. The width is $O(D/v) = 10^{-6}$. We have taken an exponential with exponent 175 in direction $x$ as the master element. This is equivalent to working in a domain with an exponential whose exponent is 350.

## 8. CONCLUSIONS

The technique presented in this work has the following properties, which have been numerically tested.

1. Good representation of interior and boundary layers without oscillations. The computed $L^2$ and $H^1$ errors show this fact.
2. Good behaviour of the scheme when $D$ decreases.
3. Computational cost.
   (a) The generation of the mesh has the same cost as that of Delaunay-type non-structured mesh generators.
   (b) The number of quadrature points in each element is greater than that used in standard methods with polynomial approximations. However, since we need fewer elements, the total number of integration points on the whole domain is equivalent to that of other methods.
   (c) The number of degrees of freedom diminishes.

Therefore the computational cost of the algorithm is similar to that of spectral and finite element methods as regards assembly of the matrix. However, concerning the solution of the algebraic system of equations, it is less.

## REFERENCES


1. O. Pironneau, *Finite Elements Methods for Fluids*, Wiley/Masson, Chichester/Paris, 1989.
2. C. Bernardi, Y. Maday and A. T. Patera, 'A new nonconforming approach to domain decomposition: the mortar element method', *Publ. Laboratoire d'Analyse Numérique*, no. R89027, Université Pierre et Marie Curie, Paris, 1990.
3. C. Bernardi, Y. Maday, C. Mavriplis and A. T. Patera, 'The mortar element methods applied to spectral discretizations', *Proc. Seventh Int. Conf. of Finite Element Methods in Flow Problems*, University of Alabama Press, Huntsville, AL, 1989, pp. 1–9.
4. C. Bernardi and Y. Maday, 'Coupling spectral and finite element methods for the Poisson equation: a review', *Proc. Seventh Int. Conf. of Finite Element Methods in Flow Problems*, University of Alabama Press, Huntsville, AL, 1989, pp. 10–19.
5. C. Canuto, M. Y. Hussaini, A. Quarteroni and T. A. Zang, *Spectral Methods in Fluid Dynamics*, Springer, New York, 1988.
6. J. C. Heinrich, 'El método de Petrov–Galerkin para flujos convectivos', *Actas I Congr. de Métodos Numéricos en Ingeniería*, ed. G. Winter and Galante, SEMNI, Barcelona, 1990, pp. 19–29.
7. J. C. Heinrich, 'On quadratic element in finite element solutions of steady-state convection-diffusion equations', *Int. j. numer. methods eng.*, **15**, 1041–1052 (1980).
8. T. J. R. Hughes and A. N. Brooks, 'A theoretical framework for Petrov–Galerkin method, with discontinuous weighting function: applications to the streamline upwind procedure', in *Finite Elements in Fluids*, Vol. 4, Wiley, London, 1982, pp. 46–65.
9. T. J. R. Hughes, M. Mallet and A. Mizukami, 'A new finite element formulation for computational fluid dynamics: II. Beyond SUPG', *Comput. Methods Appl. Mech. Eng.*, **54**, 341–355 (1986).
10. F. Olmos, 'Elementos espectrales modificados para el tratamiento numérico de la ecuación de convección–difusion', *Tesis Doctoral*, Universitat de València, 1992.
11. H. Schlichting, *Teoría de la Capa Límite*, Ediciones Urmo, Bilbao, Spain, 1975.
12. M. Van Dyke, *Perturbation Methods in Fluid Mechanics*, Parabolic, Stanford, CA, 1975.
13. J. Kevorkian and J. Cole, *Perturbation Methods in Applied Mathematics*, Springer, New York, 1981.
14. J. Otto, *Ph.D. Thesis*, Department of Computer Science, University of Colorado at Denver, 1992.
15. E. M. Ronquist, 'Optimal spectral element methods for the unsteady three-dimensional incompressible Navier–Stokes equation', *Ph.D. Thesis*, Massachusetts Institute of Technology, 1988.
16. C. Bernardi and Y. Maday, 'Spectral methods for the approximation of fourth-order problems: applications to the Stokes and Navier–Stokes equations', *Comput. Struct.*, **14**, 205–216 (1988).
17. J. E. Dennis and R. B. Schnabel, *Numerical Methods for Unconstrained Optimization and Nonlinear Equations*, Prentice-Hall, Englewood Cliffs, NJ, 1983.
18. A. Tijonov and A. Samarsky, *Ecuaciones de la Física Matemática*, MIR, Moscow, 1972.
19. C. Canuto and A. Quarteroni, 'Approximation results for orthogonal polynomials in Sobolev spaces', *Math. Comput.*, **38**, 67–86 (1982).
20. C. Canuto and A. Quarteroni, 'Variational methods in the theoretical analysis of spectral approximations', in *Spectral Methods for Partial Differential Equations*, ed. R.G. Voigt, D. Gottlieb and M.Y. Hussaini, SIAM, Philadelphia, PA, 1984, pp. 55–78.
21. R. Codina, E. Oñate, M. Cervera and K. Eckstein, 'Una formulación de Petrov–Galerkin para flujos convectivos', *Actas I Congr. de Métodos Numéricos en Ingeniería*, ed. G. Winter and Galante, SEMNI, Barcelona, 1990, pp. 134–141.
22. F. Chinesta and R. Torres, 'Modelizacón de las condiciones de contorno para la evaluación por elementos finitos del proceso de convección–difusión de un gas en recintos cerrados', *Actas I Congr. de Métodos Numéricos en Ingeniería*, ed. G. Winter and Galante, SEMNI, Barcelona, 1990, pp. 169–176.
23. F. Chinesta, R. Torres and F. Olmos, 'Modelización matemática y tratamiento numérico del proceso de convección–difusión de un gas en un recinto cuasicerrado', *An. Ing. Mec.*, Año 8, **2**, 221–227 (1990).
24. F. Chinesta, F. Olmos, R. Torres and E. Checa, 'Modified spectral element method for the convection–diffusion equation', *Proc. Non Linear Engineering Computations*, Pineridge, Swansea, 1991, pp. 629–639.
25. F. Chinesta, F. Olmos, R. Torres and E. Checa, 'Estudio cualitativo y numérico de la ecuación de convección–difusión y aproximación de la solución en una base polinomico– exponencial', *Actas XII CEDYA-II Congr. de Matemática Aplicada*, Oviedo, Spain, 1992, pp. 209–214.
26. T. J. Chung, *Finite Element Analysis in Fluid Dynamics*, McGraw- Hill, New York, 1986.
27. P. J. Davis and P. Rabinowitz, *Methods for Numerical Integration*, Academic, Orlando, FL, 1985.
28. D. Gottlieb, Y. Hussaini and S. Orszag, 'Theory and applications of spectral methods', in *Spectral Methods for Partial Differential Equations*, ed. R. G. Voigt, D. Gottlieb and M.Y. Hussaini, SIAM, Philadelphia, PA, 1984, pp. 1–54.
29. D. Gottlieb and S. Orszag, *Numerical Analysis for Spectral Methods*, SIAM, Philadelphia, PA, 1977.
30. D. W. Kelly, S. Nakazawa, O. Zienkiewicz and J. C. Heinrich, 'A note on upwinding and anisotropic balancing dissipation in finite element approximations to convective diffusion problems', *Int. j. numer. methods eng.*, **15**, 1705–1711 (1980).

31. Y. Maday, C. Mavriplis and A. T. Patera, 'Nonconforming mortar element methods: application to spectral discretizations', *Publ. Laboratoire d'Analyse Numérique*, no. R88048, Université Pierre et Marie Curie, Paris, 1988.
32. Y. Maday and A. T. Patera, 'Spectral element methods for the Navier–Stokes equation', in A. K. Noor (ed.), *State of the Art Surveys in Computational Mechanics*, ASME, New York, 1988.
33. C. Mavriplis, 'Nonconforming discretizations and "a posteriori" error estimators for adaptative spectral element techniques', *Doctoral Thesis*, Massachusetts Institute of Technology, 1989.
34. B. Mercier, *An Introduction to the Numerical Analysis of Spectral Methods*, LNP Vol. 318, Springer, New York, 1988.
35. Y. Morchoisne, 'Inhomogeneous flow calculations by spectral methods: monodomain and multidomain techniques', in *Spectral Methods for Partial Differential Equations*, SIAM, Philadelphia, PA, 1984.
36. F. Olmos, E. Checa, F. Chinesta and R. Torres, 'Nonstandard approximation on spectral techniques in convection diffusion problems', *Proc. First Eur. Computational Fluid Dynamics Conf.*, Vol. 1, 1992, pp. 75–81.
37. S. Orszag, 'Spectral methods for problems in complex geometries', *J. Comput. Phys.*, **37**, 37–70 (1980).
38. A. T. Patera, 'A spectral element method for the fluid dynamics: laminar flow in a channel expansion', *J. Comput. Phys.*, **54**, 468–488 (1984).
39. P. J. Roache, *Computational Fluid Dynamics*, Hermosa, Albuquerque, NM, 1972.
40. P. A. B. Sampaio, 'A Petrov–Galerkin modified operator formulation for convection–diffusion problems', *Int. j. numer. methods eng.*, **30**, 331–347 (1990).
41. G. Strang and G. Fix, *An Analysis of the Finite Element Method*, Prentice-Hall, Englewood Cliffs, NJ, 1973.
42. T. Strouboulis and J. T. Oden, 'A posteriori error estimation of finite element approximations in fluid mechanics', *Comput. Methods Appl. Mech. Eng.*, **78**, 201–242 (1990).
43. W. G. Szimczak, 'An analysis of viscous splitting and adaptivity for steady-state convection–diffusion problems', *Comput. Methods Appl. Mech. Eng.*, **78**, 311–354 (1988).
44. G. Touzot and G. Dhatt, *Une Présentation de la Méthode des Eléments Finis*, Maloine, 1984.
45. R. Wait and A. R. Mitchel, *Finite Element Analysis and Applications*, Wiley, Chichester, 1985.
46. O. C. Zienkiewicz, R. H. Gallagher and P. Wood, 'Newtonian and non-Newtonian viscous incompressible flow finite element solution', *Proc. 2nd Conf. on the Mathematics of Finite Elements and Applications*, Academic, London, 1976, pp. 235–267.